Reduced Graphene Oxide (rGO)-Wrapped Fullerene (C_{60}) Wires

Jieun Yang,[†] Mihee Heo,[†] Hyo Joong Lee,[‡] Su-Moon Park,[†] Jin Young Kim,[†,*] and Hyeon Suk Shin[†,*]

[†]Interdisciplinary School of Green Energy and KIER-UNIST Advanced Center for Energy, Ulsan National Institute of Science & Technology (UNIST), UNIST-gil 50, Ulsan 689-805, Korea and [‡]Department of Chemistry, Chonbuk National University, 567 Baekje-deokjin-gu, Jeonju-si, Jeollabuk-do 561-756, Korea

ABSTRACT The assembly of reduced graphene oxide (rGO) and fullerene (C_{60}) into hybrid (rGO/C_{60}) wires was successfully performed by employing the liquid−liquid interfacial precipitation method. The rGO sheets spontaneously wrapped C_{60} wires through the $\pi-\pi$ interaction between rGO and C_{60}. Structural characterization of the rGO/C_{60} wires was carried out by using UV/visible spectroscopy, scanning electron microscopy, and transmission electron microscopy. FET devices with rGO/C_{60} wires were fabricated to investigate their electrical properties. The $I_{ds}-V_g$ curves of the hybrid wires exhibited p-type semiconducting behavior both in vacuum and in air, indicating hole transport through rGO as a shell layer, whereas pure C_{60} wires and rGO sheets showed n-type and ambipolar behaviors, respectively, under vacuum. Possible application of the fabricated wires, such as photovoltaic devices, was also demonstrated.

KEYWORDS: reduced graphene oxide · field effect transistor · fullerene wires · charge transfer · photovoltaic device

Organic and inorganic hybrid materials with carbon allotropes such as fullerene and carbon nanotubes (CNTs) have attracted much attention. The charge transfer at the interface of these hybrid materials can show a synergistic effect to induce interesting properties that are different from those of each component. For example, CNTs functionalized with light-sensitive materials such as CdSe and TiO_2 nanoparticles showed variation of conductance at a specific wavelength in field effect transistor (FET) devices due to photoinduced charge transfer from the nanoparticles to CNTs.[1−3] Wavelength-selective silencing of photoconductivity in Au nanoparticle-coated fullerene wires due to electron transfer by the surface plasmon resonance (SPR) of Au nanoparticles was also reported.[4] These approaches have opened possibilities for application with photodetectors and sensors.

On the other hand, the charge transfer can be a driving force for the formation of hybrid materials. Wakahara *et al*. speculated that the strong charge transfer between C_{60} and ferrocene (Fc) at 782 nm enabled the interaction of the nearest C_{60}−Fc pair, which is possibly a driving force for the formation of C_{60}/Fc nanosheets.[5] In addition, hybrid materials consisting of only carbon nanomaterials, such as CNTs coated with C_{60} molecules, could be prepared by noncovalent functionalization.[6,7] An interesting result was that hybrid materials of higher fullerene (C_{70}) with an ellipsoidal shape and single-walled carbon nanotubes (SWNTs) showed efficient electron transfer due to improved interaction between C_{70} and the sidewalls of the SWNTs. A photoelectrochemical device fabricated with the hybrid materials exhibited the highest IPCE value (26%) among analogous SWNT-based photoelectrochemical devices.[8]

Graphene enables interactions with other organic and inorganic components for hybrid materials through $\pi-\pi$ interaction, which is efficient due to its large surface area.[9−11] Noncovalent bonding such as hydrogen bonding, van der Waals interaction, and $\pi-\pi$ interaction provides a simpler process for preparation of hybrid materials than covalent bonding. In particular, it is anticipated that reduced graphene oxide (rGO) with functional groups can be exploited to develop many hybrid structures, because it is soluble in various solvents.[12,13] Indeed, some recent efforts have been made to prepare graphene hybrid materials. For instance, *N*,*N*′-dioctyl-3,4,9,10-perylenedicarboximide (PDI) wire with aromatic structures has been coated by rGO *via* the $\pi-\pi$ interaction.[14] The charge transfer between n-type PDI and rGO in the hybrid wires could be applicable to organic photovoltaic devices. In addition, electrostatic interaction between an aromatic peptide wire with positive charges and rGO with negative charges enabled peptide/rGO core/shell wires. Application of biomolecules is limited due to their poor electrical property and low thermal stability, whereas the rGO-coated peptide wire became conductive and could be used for supercapacitor electrodes.[12]

* Address correspondence to shin@unist.ac.kr; jykim@unist.ac.kr.

Received for review August 11, 2011 and accepted September 21, 2011.

Published online September 21, 2011
10.1021/nn203073q

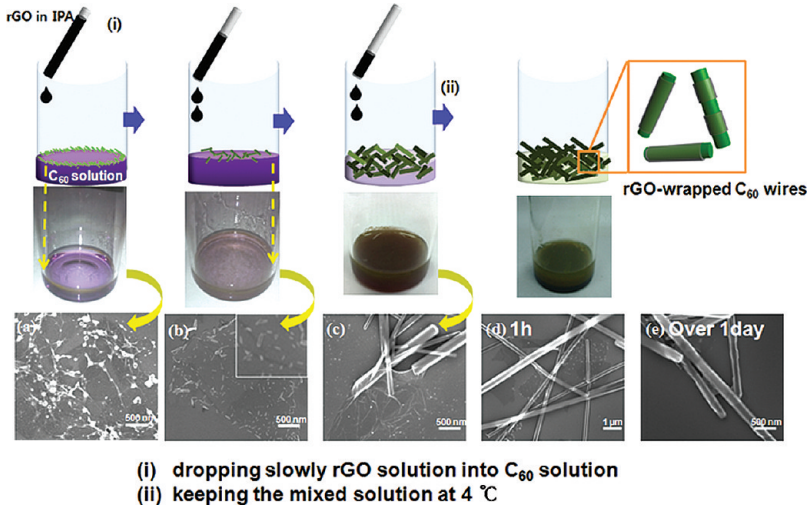

Figure 1. Schematic illustration and SEM images (a–e) showing steps of formation of rGO-wrapped C_{60} wires.

Herein, we report the assembly of rGO and C_{60} into hybrid wires by employing the liquid–liquid interfacial precipitation (LLIP) method. The process of the assembly was carefully investigated by scanning electron microscopy (SEM) and transmission electron microscopy (TEM), and finally the formation of rGO-wrapped C_{60} wires was observed. It was identified from UV/vis spectroscopy that the driving force of the assembly is the $\pi-\pi$ interaction between rGO and C_{60}. Interestingly, rGO/C_{60} hybrid wires showed a p-type semiconducting behavior in field effect transistor devices both in a vacuum and in air, whereas rGO and C_{60} displayed ambipolar and n-type semiconducting behaviors in a vacuum, respectively. These results indicate electron transfer from rGO to C_{60}. Furthermore, we explored some applications such as photoluminescence and a solar cell based on charge transfer.

RESULTS AND DISCUSSION

The rGO-wrapped C_{60} wires (rGO/C_{60}) were prepared by liquid–liquid interfacial precipitation.[15–17] This method is suitable for obtaining a large quantity of C_{60} wires. It is noted that C_{60} wires prepared by LLIP have higher strength and better electrical conductivity than C_{60} wires prepared by solvent evaporation, because the C_{60} molecules in LLIP are confined within the very narrow space of the interface of two solvents, and thus they have a smaller intermolecular distance between the C_{60} molecules.[17]

An rGO aqueous solution with a concentration of 0.5 wt % was dispersed in isopropyl alcohol (IPA). The size distribution of the rGO sheets was between a few hundred nm and 2 μm by atomic force microscopy (AFM) (Figure S1). Meanwhile, C_{60} powder was dissolved in *m*-xylene to prepare a saturated solution. The rGO IPA solution was gently added into a vial including the C_{60} *m*-xylene solution to form a precipitate at the liquid–liquid interface, wherein the upper phase is the rGO in the IPA and the lower phase is the C_{60} *m*-xylene solution. Once nucleation of the C_{60} wires starts to occur at the liquid–liquid interface, green precipitates were observed at the interface along the vial surface (Figure 1a). By continuously adding the rGO solution into the C_{60} solution, the C_{60} solution was gradually covered with nanorods with a length in the range 30–200 nm. (Figure 1b is a SEM image 2 min after rGO solution was added into the C_{60} solution.) Note that the C_{60} particles and nanorods are attached to rGO sheets as shown in Figure 1a and b. After dropping all of the rGO solution, the apparent interface of IPA and *m*-xylene disappeared and C_{60} wires were observed. The C_{60} wires were partially wrapped with rGO sheets, and their lengths were less than a few micrometers (Figure 1c). To promote the growth of C_{60} wires wrapped with rGO, the vial was capped and left at 4 °C in a refrigerator. The color of the precipitates changed to dark green after being held at 4 °C for a certain amount of time. Although the C_{60} wires are not fully wrapped with rGO sheets after 1 h, the length of the C_{60} wires was more than 10 μm (Figure 1d). It was observed that the C_{60} wires were fully wrapped with rGO sheets after 1 day (Figure 1e). Free rGO sheets were removed by centrifugation at 500 rpm. As a control experiment, C_{60} wires were prepared by LLIP using pure IPA without rGO. As soon as IPA was added to the C_{60} solution, green precipitates of only C_{60} particles were also observed at the interface of the C_{60} solution and IPA (Figure S2(a)). After dropping IPA for 2 min, long C_{60} wires more than a few micrometers were observed (Figure S2(b)), whereas short C_{60} nanorods on rGO sheets were observed in case of adding the rGO IPA solution in Figure 1b. This means that the growth of C_{60} wires gets slow in the presence of rGO, possibly due to the interaction between rGO and C_{60}. After dropping all of the IPA, the mixed

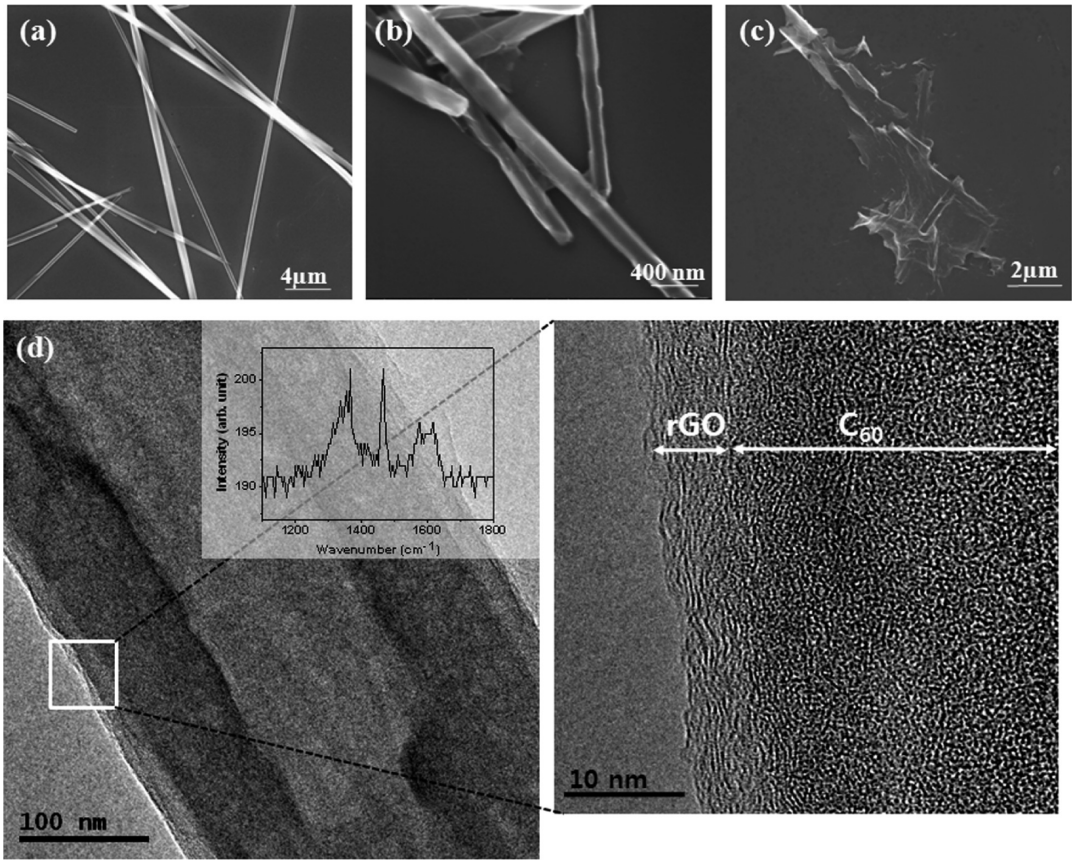

Figure 2. SEM images of (a) only C_{60} wires, (b) rGO/C_{60} wires, and (c) rGO after dissolving C_{60} wires in *m*-xylene. (d) TEM images of a rGO/C_{60} wire. The magnified image in (d) shows rGO layers. The inset in (d) shows a Raman spectrum of a rGO/C_{60} wire in which bands of rGO and C_{60} were observed.

solution was capped and left at 4 °C. After 1 h, the C_{60} wires with the length of more than 10 μm were formed (Figure S2(c)).

Figure 2a shows a SEM image of pure C_{60} wires with a diameter range of 200−800 nm. Figure 2b shows the rGO/C_{60} wires left at 4 °C for 1 day. C_{60} in the rGO/C_{60} wires can be selectively dissolved in *m*-xylene to confirm the presence of the rGO attached to the C_{60} wires. Figure 2c shows the rGO shells that remained after selective dissolution of the C_{60} wires in *m*-xylene. The wrapping of rGO was also confirmed by TEM images in Figure 2d. The magnified image in Figure 2d obviously shows a C_{60} core and rGO shell with a layered structure. As a control experiment, we measured HR-TEM images of C_{60} wires only before wrapping rGO sheets and confirmed that there are no layered structures similar to Figure 2d (Figure S3). Also, the Raman spectrum of a rGO/C_{60} wire in the inset of Figure 2d confirms the existence of rGO and C_{60}: D and G bands around 1350 and 1600 cm^{-1} for rGO and $A_g(2)$ mode at 1469 cm^{-1} for C_{60}. As a control experiment, C_{60} wires were first prepared by LLIP and then immersed into the rGO solution. Most of the rGO sheets did not wrap the C_{60} wires, but were randomly laid on them (Figure S4). In parts of the sample, some small rGO sheets wrapped the wires.

Figure 3a−c show UV−vis spectra of C_{60} wires, rGO, and rGO/C_{60} wires, respectively. The spectrum of the C_{60} wires in Figure 3a shows two bands, at 270 and 340 nm. These two bands correspond to the strongly allowed electronic transitions, $6^1T_{1u}-1^1A_g$ and $3^1T_{1u}-1^1A_g$, respectively.[18] Since the red shift of the band at 340 nm is correlated with interactions between C_{60} and different molecules, the band is an important indicator for the interaction of fullerene and aromatic rings or fullerene and a polymer.[19] Note that the band at 340 nm in the C_{60} wires shifted to 380 nm in the rGO/C_{60} wires (Figure 3c). The large shift of 40 nm is correlated to the strong delocalization of the π electron system of rGO sheets in the vicinity of the C_{60} wires. This result means that the $\pi-\pi$ interaction is the main driving force for the formation of the rGO/C_{60} wires. The $\pi-\pi$ stacking reduces the surface energy of the molecules. Furthermore, the $\pi-\pi$ interaction was observed even in green precipitates formed as soon as the rGO IPA solution was dropped into the C_{60} solution, as presented in Figure 1a.

In Figure S5(a), the UV/vis spectrum shows an absorption band at 390 nm, which is identical to the result by the $\pi-\pi$ interaction provided in Figure 3c. This means that the C_{60} precipitates (particles) were attached to the rGO sheets. The absorption band at

390 nm remains after the solution was left at 4 °C for 1 h (Figure S5(b)). As a control experiment, the growth of C_{60} wires by adding pure IPA into the C_{60} solution was investigated, and the results are given in Figure S5(c) and (d). The C_{60} precipitates (particles) and wires showed an absorption band around 340 nm in the UV/vis spectra. Therefore, the $\pi-\pi$ interaction between C_{60} and rGO sheets occurs from the initial step where the IPA solution with rGO sheets is added to the C_{60} solution.

To understand charge transfer in the rGO/C_{60} wires, the energy levels of rGO and C_{60} were investigated. It is known that GO has a band gap of ~2.2 eV, and the band gap of a few-layer rGO sheet can be controlled between 0.5 and 1.4 eV depending on the extent of reduction by the applied thermal reduction process.[20]

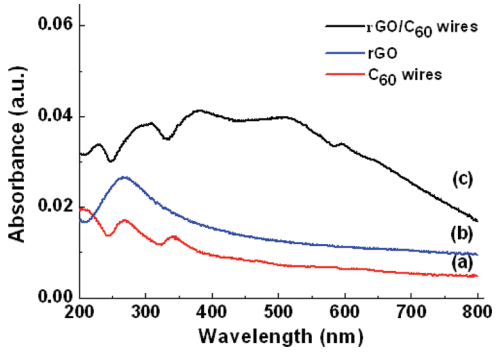

Figure 3. UV/vis spectra of (a) C_{60} wires, (b) rGO, and (c) rGO/C_{60} wires. The spectra were measured after spin-coating the solutions on quartz substrates.

In this study, cyclic voltammetry (CV) and photoelectron spectroscopy were employed to measure LUMO and Fermi levels of rGO. The LUMO energy level of rGO was calculated to be 3.65 eV using a well-defined reduction peak in the cyclic voltammogram (Figure S6). The Fermi level of rGO was 4.8 eV from the photoelectron spectrum (Figures S7). The above LUMO and Fermi levels are very similar to the results of previous reports: the LUMO level of imidazole-modified GO was 3.6 eV by CV and the Fermi level of rGO was 4.88 eV by photoelectron spectroscopy or 4.7 eV by Kelvin probe force microscopy.[21−23] Therefore, the band gap of rGO in this study appears to be slightly larger than 1.15 eV. This indicates that rGO can be used as an absorber of visible light. (See the example application of a photovoltaic device later in this paper.) In the case of C_{60}, it is known that the LUMO is 4.3 eV and the HOMO is 6.6 eV.[24] Actually, the Fermi level of C_{60} wires was 5.1 eV by photoelectron spectroscopy (Figure S8). Consequently, electrons can transfer from rGO to C_{60} in rGO/C_{60} wires because the Fermi level of rGO is higher than that of C_{60}.

To investigate the electrical properties, we fabricated FET devices of rGO/C_{60} wires, rGO sheets, and C_{60} wires. Figure 4 shows optical images and $I-V_g$ curves of the FET devices. Most of the measurements were performed under vacuum to remove the influence of oxygen. Also, an annealing process at 325K for 8 h under vacuum before electrical measurements was carried out to remove adsorbed O_2 and H_2O on the samples. The rGO sheets exhibited ambipolar

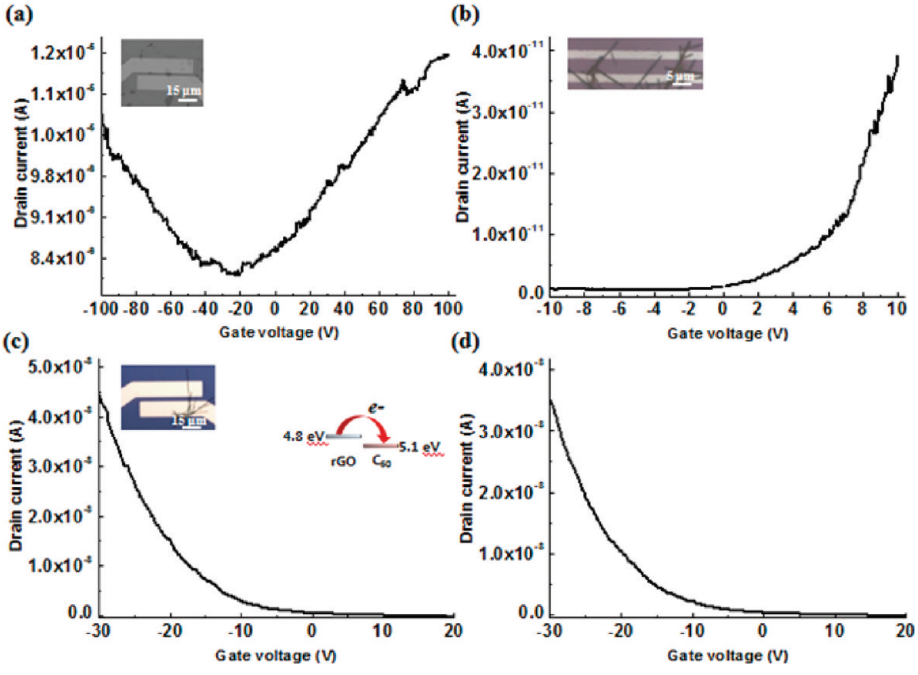

Figure 4. $I_{ds}-V_g$ of (a) rGO in vacuum, (b) C_{60} wires in vacuum, (c) rGO/C_{60} wires in ambient, and (d) rGO/C_{60} wires in a vacuum. The bias voltage, V_{ds}, was 1 V for (a) and 10 V for (b), and 5 V for (c) and (d). Optical images of the corresponding devices are shown in the insets of (a), (b), and (c).

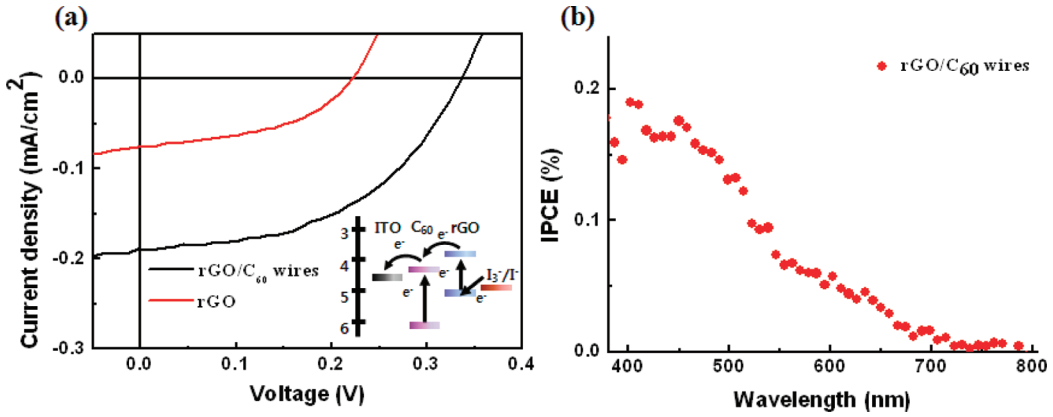

Figure 5. (a) *J*–*V* curves of rGO and rGO/C_{60} wires. (b) IPCE spectrum of rGO/C_{60} wires.

characteristics under vacuum, which is identical to previous results[25,26] (Figure 4a). However, the Dirac point appeared near $V_g = -20$ V. It is considered that the reduction process using ammonia solution and hydrazine induced the shift of a Dirac point to negative gate voltage, *i.e.*, an n-doping effect, due to remaining N atoms. This was confirmed from an elemental analysis of rGO, which included N atoms of 2.81 wt % (Table S1). The FET of the C_{60} wires showed a typical n-type behavior under vacuum (Figure 4b). This result is consistent with a previous report.[15] On the other hand, the rGO/C_{60} wires showed p-type behaviors in air as well as under vacuum, as shown in Figure 4c and d, indicating hole transport through rGO. These electrical properties reveal that the p-type behaviors of the rGO/C_{60} wires reveal that rGO sheets are heavily p-doped due to electron transfer from rGO to C_{60}, as indicated in the inset of Figure 4c. The hole mobility (0.04 cm^2/(V s)) for the rGO/C_{60} wire in Figure 4c is lower than that (0.6 cm^2/(V s)) for rGO sheets in Figure 4a. The lower mobility in rGO/C_{60} wires might be due to many junctions between rGO sheets on C_{60} wires. Further, this study indicates that rGO/C_{60} wires are not sensitive to O_2 and H_2O molecules and are stable even in air.

To further understand interesting optoelectronic behaviors of the rGO/C_{60} wires, such as the photocurrent generation and PL quenching, photovoltaic devices were fabricated. To our best knowledge, rGO has so far been used as an electron acceptor instead of C_{60} in organic photovoltaic devices.[27,28] However, our results clearly indicate that rGO can act as a sensitizer since the photoexcited electron from rGO is injected into the LUMO energy level of C_{60}, as shown in the inset of Figure 5a. The rGO/C_{60} wires are regenerated by the redox system (I_3^-/I^-) at the counter electrode *via* electron migration through the external load. The *J*–*V* characteristics of the devices using rGO and rGO/C_{60} wires under simulated AM 1.5 G illumination are shown in Figure 5a, while the corresponding numerical results are summarized in Table 1. Replacing rGO with rGO/C_{60} wires caused a significant enhancement of short-circuit current (J_{SC}) from 0.07 to 0.19 mA cm^{-2}. The observed current increase can be interpreted that the photoinduced electrons are efficiently transferred from the rGO to C_{60} under light irradiation. (Photoinduced charge transfer was observed in photoluminescence measurements in Figure S9.)

TABLE 1. Solar Cell Characteristics of rGO and rGO/C_{60} Wires

	J_{sc} (mA/cm^2)	V_{oc} (V)	FF (%)	E_{ff} (%)
rGO	0.07	0.18	0.45	0.006
rGO/C_{60} wire	0.19	0.33	0.50	0.03

The incident photon to current efficiency (IPCE) was obtained to confirm the photocurrent generation in the solar cell with the rGO/C_{60} wires. As shown in Figure 5b, the photocurrent generation of the rGO/C_{60} wires is obvious. It is noted that both rGO and C_{60} in the rGO/C_{60} wires contribute to the photocurrent generation since the IPCE spectral feature from 400 to 700 nm is attributable to the contribution of electrons generated from the photoexcitation of both rGO and C_{60}. As a result, this enables significant enhancement of J_{sc} in the solar cell with rGO/C_{60} wires. Even though the performance of the rGO/C_{60} wires still appears relatively low, we highlight that this study is the first report on rGO as a sensitizer for the photovoltaic devices, which should open up new strategies for the development of this field.

CONCLUSION

In conclusion, rGO-wrapped C_{60} wires were successfully prepared *via* the LLIP method. The main driving force for the assembly of rGO sheets and C_{60} wires is the π–π interaction. The rGO-wrapped C_{60} wires exhibited p-type semiconducting behaviors in air and in a vacuum, indicating charge transfer between rGO and C_{60} and hole transport through rGO. Furthermore, we presented interesting applications such as a photovoltaic device albeit with relatively low efficiency. The assembly of carbon nanomaterials and the electron transfer at interfaces induced interesting and unprecedented

properties. Therefore, future efforts will focus not only on new graphene-based nanostructures or hybrid materials with functionalized graphene but also on charge transfer at interfaces in newly designed hybrids.

EXPERIMENTAL METHODS

Preparation of Reduced Graphene Oxide. Graphite oxide was synthesized by the modified Hummers method and exfoliated to give a brown dispersion of graphene oxide under ultrasonication.[29−31] The resulting graphene oxide (GO) is negatively charged over a wide pH range since the GO sheet has chemical functional groups such as carboxylic acids. GO suspensions were reduced by hydrazine solution (35 wt % in water, Aldrich) to convert into reduced graphene oxide. The as-prepared negatively charged GO suspension (5.0 mL) was mixed with 5.0 mL of hydrazine solution and 35.0 mL of ammonia solution (28−30%, Samchun) in a 20 mL glass vial. After stirring for a few minutes, the vial was put in a water bath at 95 °C for 1 h.

Preparation of rGO/C_{60} Wires. Fullerene (C_{60}) powder (Sigma Aldrich, 99%) was dissolved in *m*-xylene to make a solution of 2 mg/mL, and the C_{60} solution was kept in a glass vial. The rGO aqueous solution (50 μL) was added into 2 mL of isopropyl alcohol. The rGO IPA solution was then gently added into the glass vial containing the C_{60} solution to form a liquid−liquid interface where the upper phase is IPA and the lower phase is the *m*-xylene solution of C_{60}. The vial was loosely capped and kept at 4 °C over 1 day. To remove free rGO sheets, the solution was centrifuged at 500 rpm. The centrifugation with IPA was repeated a few times to wash the hybrid rGO/C_{60} wires. The wires obtained were characterized by HR-TEM (JEOL, JEM-2100F, 200 KV). The exposure time was 0.5 s, and the current density was 55 pA/cm^2 in magnified images.

Measurement of UV/Vis Spectra and Photoluminescence Spectra. rGO/C_{60} wires were spin-coated at 1000 rpm on a quartz plate. The rGO/C_{60} wires coated on the quartz plate were dried at 130 °C in a vacuum for 1 h. Then, absorption and photoluminescence spectra were measured by a UV/vis spectrometer (Cary 5000 model, Varian) and a fluorometer (Cary Eclipse model, Varian), respectively.

Measurement of LUMO and Fermi Levels. To investigate the LUMO energy level of rGO, the cyclic voltammogram of rGO was measured by using a standard three-electrode system, which consists of a glassy carbon as the working electrode, a platinum mesh as the counter electrode, and a silver wire as the reference electrode. Acetonitrile containing 0.1 M tetrabutylammonium hexafluorophosphate ($TBAPF_6$) was used as the supporting electrolyte. The LUMO energy level of rGO was calculated according to the following equations.

$$Fc/Fc^{+} : 0.595\ V\ vs\ Ag\ wire$$

$$LUMO\ (eV) = -4.8 - (E_{onset} - E_{Fc/Fc+})$$

Photoelectron spectroscopy (surface analyzer model AC-2, RIKEN KEIKI) was used to determine the Fermi energy level of rGO. This is an analyzer for detecting low-energy electrons emitted from a solid surface in air by irradiating UV light. The threshold energy of photoelectron emission is called the Fermi level, HOMO level or ionization potential, or work function.

Fabrication of FET Devices. The FET devices were fabricated by dropping solutions of C_{60} wires, rGO, and rGO-wrapped C_{60} wires on prepatterned source and drain electrodes. The prepatterned electrodes were defined on SiO_2/Si (300 nm thick SiO_2 layer on a highly doped p-type Si(100)) substrates by addressing Cr (5 nm)/Au (20 nm) electrodes by using a conventional photolithography process (photoresist: AZ5214). The channel length between source and drain electrodes was 4 μm. Electrical transport properties were measured by using a semiconductor analyzer (Keithley 4200).

Fabrication of Solar Cells. The photovoltaic solar cells with the configuration of indium tin oxide (ITO)/rGO-C_{60} wires/electrolyte/Pt electrode were fabricated. Before the device fabrication, the ITO-coated glass substrate was cleaned by ultrasonic treatment using detergent, deionized water, acetone, and isopropyl alcohol in sequence and dried in an oven for 24 h. The rGO-wrapped C_{60} wires were spin-coated at 1000 rpm for 30 s onto the cleaned ITO substrate repeatedly. The Pt-coated FTO, used as a counter electrode, was prepared by sputtering on an FTO glass followed by heating at 450 °C in air for 1 h. The rGO-wrapped C_{60} wires coated on ITO and Pt counter electrodes were assembled into a sealed sandwich-type cell by heating with a hot melt of 50 μm thick sealing tapes that served as a spacer between the electrodes. A drop of the electrolyte solution was placed on a drilled hole in the counter electrode of the cell and was driven into the cell by means of vacuum backfilling. The hole was sealed using additional sealant and a cover glass (0.1 mm thick). The redox electrolyte consisted of 0.04 M LiI, 0.02 M I_2, 0.5 M 1-hexyl-2,3-dimethylimidazolium iodine, and 0.5 M 4-*tert*-butylpyridine in acetonitrile. Photovoltaic measurements were recorded by employing a Keithley 2400 digital source meter. Solar cell performance was measured by utilizing an Air Mass 1.5 G (AM 1.5 G) solar simulator with an irradiation intensity of 100 mW cm^{-2} under ambient conditions. External quantum efficiency measurements were obtained using the PV Measurements OE system with monochromatic light from a xenon lamp. The monochromatic light intensity was calibrated with a Si photodiode and chopped at 4 Hz.

Acknowledgment. This work was supported by the WCU (World Class University) program and by the Basic Science Research Program through the National Research Foundation funded by MEST of Korea (R31-2008-000-20012-0 and 2011-0013601).

Supporting Information Available: AFM image of rGO, SEM images of C_{60} precipitates and wires, CV curve of rGO, photoelectron spectrum of rGO and C_{60}, and photoluminescence of rGO and rGO/C_{60}. This material is available free of charge via the Internet at http://pubs.acs.org.

REFERENCES AND NOTES

1. Hu, L.; Zhao, Y. L; Ryu, K.; Zhou, C.; Stoddart, J. F. Light-Induced Charge Transfer in Pyrene/CdSe-SWNT Hybrids. *Adv. Mater.* **2008**, *20*, 939–946.
2. Zhao, Y.-L.; Stoddart, J. F. Noncovalent Functionalization of Single-Walled Carbon Nanotuebes. *Acc. Chem. Res.* **2009**, *42*, 1161–1171.
3. Liu, S.; Li, J.; Shen, Q.; Cao, Y.; Guo, X.; Zhang, G.; Feng, C.; Zhang, J.; Liu, Z.; Steigerwald, M. L.; *et al.* Mirror-Image Photoswitching of Individual Single-Walled Carbon Nanotube Transistors Coated with Titanium Dioxide. *Angew. Chem., Int. Ed.* **2009**, *48*, 4759–4762.
4. Yang, J.; Lim, H.; Choi, H. C.; Shin, H. S. Wavelength-Selective Silencing of Photocurrent in Au-Coated C_{60} Wire Hybid. *Chem. Commun.* **2010**, *46*, 2575–2577.
5. Wakahara, T.; Sathish, M.; Miyazawa, K.; Hu, C.; Tateyama, Y.; Nemoto, Y.; Sasaki, T.; Ito, O. Preparation and Optical Properties of Fullerene/Ferrocene Hybrid Hexagonal Nanosheet and Large-Scale Production of Fullerene Hexagonal Nanosheets. *J. Am. Chem. Soc.* **2009**, *131*, 9940–9944.
6. Sandanayaka, A. S. D.; Maligaspe, E.; Hasobe, T.; Ito, O.; D'Souza, F. Diameter Dependent Electron Transfer in Supramolecular Nanohybrids of (6,5)- or (7,6)-Enriched Semiconducting SWNT as Donors and Fullerene as Acceptor. *Chem. Commun.* **2010**, *46*, 8749–8751.
7. Arnold, M. S.; Zimmerman, J. D.; Renshaw, C. K.; Xu, X.; Lunt, R. R.; Austin, C. M.; Forrest, S. R. Broad Spectral Response Using Carbon Nanotube/Organic Semiconductor/C_{60} Photodetectors. *Nano Lett.* **2009**, *9*, 3354–3358.
8. Umeyama, T.; Tezuka, N.; Seki, S.; Matano, Y.; Nishi, M.; Hirao, K.; Lehtivuori, H.; Tkachenko, N. V.; Lemmetyinen, H.;

Nakao, Y.; *et al*. Selective Formation and Efficient Photocurrent Generation of [70]Fullerene−Single-Walled Carbon Nanotube Composites. *Adv. Mater.* **2010**, *22*, 1767–1770.
9. Stankovich, S.; Dikin, D. A.; Dommett, G. H. B.; Kohlhaas, K. M.; Zimney, E. J.; Stach, E. A.; Piner, R. D.; Nguyen, S. T.; Rouff, R. S. Graphene- Based Composite Materials. *Nature* **2006**, *442*, 282–286.
10. Geim, A. K.; Novoselov, K. S. The Rise of Graphene. *Nat. Mater.* **2007**, *6*, 183–191.
11. Geim, A. K. Graphene: Status and Prospects. *Science* **2009**, *324*, 1530–1534.
12. Han, T. H.; Lee, W. J.; Lww, D. H.; Kim, J. E.; Choi, E.-Y.; Kim, S. O. Peptide/Graphene Hybid Assembly into Core/Shell Nanowires. *Adv. Mater.* **2010**, *22*, 2060–2064.
13. Loh, K. P.; Bao, Q.; Ang, P. K.; Yang, J. The Chemistry of Graphene. *J. Mater. Chem.* **2010**, *20*, 2277–2289.
14. Wang, W.; Goh, E. M.; Manga, K. K.; Bao, Q.; Yang, P.; Loh, K. P. Graphene as Atomic Template and Structural Scaffold in the Synthesis of Graphene-Organic Hybrid Wire with Photovoltaic Properties. *ACS Nano* **2010**, *4*, 6180–6187.
15. Ogawa, K.; Kato, T.; Ikegami, A.; Tsuji, H.; Aoki, N.; Ochiai, Y. Electrical Properties of Field-Effect Transistors Based on C_{60} Nanowhiskers. *Appl. Phys. Lett.* **2006**, *88*, 112109.
16. Minato, J.-I.; Miyazawa, K. Solvated Structure of C_{60} Nanowhiskers. *Carbon* **2005**, *43*, 2837–2841.
17. Miyazawa, K.; Kuwasaki, Y.; Obayashi, A.; Kuwabara, M. C_{60} Nanowhiskers Formed by the Liquid-Liquid Interfacial Precipitation Method. *J. Mat. Res.* **2002**, *17*, 83–88.
18. Bensasson, R. V.; Bienvenue, E.; Dellinger, M.; Leach, S.; Seta, P. C_{60} in Model Biological Systems. A Visible-UV Absorption Study of Solvent-Dependent Parameters and Solute Aggregation. *J. Phys. Chem.* **1994**, *98*, 3492–3500.
19. Chubarova, E. V.; Melenevskaya, E. Y. Analysis of Interaction in Fullerene-solvent-polymer System by UV-spectroscopy. *Fullerenes, Nanotubes Carbon Nanostruct.* **2008**, *16*, 640–643.
20. Chang, H.; Sun, Z.; Yuan, Q.; Ding, F.; Tao, X.; Yan, F.; Zheng, Z. Thin Film Field-Effect Phototransistors from BandGap-Tunable, Solution-Processed, Few-Layer Reduced Graphene Oxide Films. *Adv. Mater.* **2010**, *22*, 4872–4876.
21. Karousis, K.; Economopoulos, S. P.; Sarantopoulou, E.; Tagmatarchis, N. Porphyrin Counter Anion in Imidazolium-Modified Graphene Oxide. *Carbon* **2010**, *48*, 854–860.
22. Kong, B.-S.; Geng, J.; Jung, H.-T. Layer-by-Layer Assembly of Graphene and Gold Nanoparticles by Vacuum Filtration and Spontaneous Reduction of Gold Ions. *Chem. Commun.* **2009**, *16*, 2174–2176.
23. Liu, J.; Yin., Z.; Cao, X.; Lin, A.; Xie, L.; Fan, Q.; Boey, F.; Zhang, H.; Huang, W. Bulk Heterojunction Polymer Memory Devices with Reduced Graphene Oxide as Electrodes. *ACS Nano* **2010**, *4*, 3987–3992.
24. Veenstra, S. C.; Heeres, A.; Hadzhoannou, G.; Sawatzky, G. A.; Jonkman, H. T. On Interface Dipole Layers between C_{60} and Ag or Au. *Appl. Phys. A: Mater. Sci. Process* **2002**, *75*, 661–666.
25. Li, X.; Wang, H.; Robinson, J. T.; Sanchez, H.; Diankov, G.; Dai, H. Simultaneous Nitrogen Doping and Reduction of Graphene Oxide. *J. Am. Chem. Soc.* **2009**, *131*, 15939–15944.
26. Eda, G.; Fanchini, G.; Chhowalla, M. Large-Area Ultrathin Films of Reduced Graphene Oxide as a Transparent and Flexible Electronic Materials. *Nat. Nanotechnol.* **2008**, *3*, 270–274.
27. Liu, Z.; Liu, Q.; Huang, Y.; Ma, Y.; Yin, S.; Zhang, X.; Sun, W.; Chen, Y. Organic Photovoltaic Devices Based on a Novel Acceptor Material: Graphene. *Adv. Mater.* **2008**, *20*, 3924–3930.
28. Liu, Q.; Liu, Z.; Zhang, X.; Zhang, N.; Yang, L.; Yin, S.; Chen, Y. Organic Photovoltaic Cells Based on an Acceptor of Soluble Graphene. *Appl. Phys. Lett.* **2008**, *92*, 223303.
29. Hummers, W. S.; J. R.; Offeman, R. E. Preparation of Graphitic Oxide. *J. Am. Chem. Soc.* **1958**, *80*, 1339.
30. Li, D.; Muller, M. B.; Gilje, S.; Kaner., R. B; Wallace, G. G. Processable Aqueous Dispersions of Graphene Nanosheets. *Nat. Nanotechnol.* **2008**, *3*, 101–105.
31. Eda, G.; Chowalla, M. Chemically Derived Graphene Oxide: Towards Large-Area Thin-Film Electronics and Optoelectronics. *Adv. Mater.* **2010**, *22*, 2392–2415.